Applied Geochemistry 149 (2023) 105570

Contents lists available at ScienceDirect

Applied Geochemistry

journal homepage: www.elsevier.com/locate/apgeochem

Granite alteration as the origin of high lithium content of groundwater in southeast Hungary

Krisztián Jancsek [a], Patrick Janovszky [b], Gábor Galbács [b], Tivadar M. Tóth [a,*]

[a] Department of Mineralogy, Geochemistry and Petrology, University of Szeged, Egyetem Street 2, 6722, Szeged, Hungary
[b] Department of Inorganic and Analytical Chemistry, University of Szeged, Dóm Square 7, 6720, Szeged, Hungary

ARTICLE INFO

Editorial handling by: Patrice de Caritat

Keywords:
Lithium
Geothermal water
Chloritisation
Granite alteration
Laser-induced breakdown spectroscopy (LIBS)

ABSTRACT

The study aimed to find the origin of the high lithium content of groundwater in southeast Hungary. To be concerned with assessing the economic potential of lithium in these waters, it is necessary to investigate the lithium-releasing geochemical processes. For this purpose, granite and pegmatite samples were analysed for lithium content and alteration from various Battonya Complex locations. The key alteration processes are the chloritisation of biotite and the sericitisation of feldspar, which are hypothesised to mobilise Li from minerals into the geothermal waters. Whole-rock analyses show that the 36 ppm Li concentration in one sample (S1) exceeded the average crustal Li concentration (~20 ppm), while three samples have near-average crustal concentrations. The Li content of rock samples decreases along with the increasing intensity of alteration. The Li concentration of biotite, muscovite, chlorite, feldspar and quartz from granites and pegmatite was measured using laser-induced-breakdown-spectrometry (LIBS). A total of 180 data points were analysed. Biotite and muscovite of the relatively fresh granites contain Li up to ~3800 and ~2500 ppm, respectively. Chloritisation is a hydrothermal alteration process in granites that can be described by the following reaction: biotite + plagioclase → chlorite + epidote + titanite + muscovite. As a function of chloritisation, Li concentration decreases two- and three orders of magnitude from biotite to chlorite in the more altered cases. A similar trend is observed for muscovite in parallel. Feldspars have Li of 17–141 ppm, while there is no correlation between the Li content of feldspars and the degree of alteration. Quartz contains constant low concentrations around the 1 ppm detection limit, with one outlier value of 48 ppm. Chloritisation of biotite is a possible explanation for the high Li content of the geothermal waters in the study area and possibly elsewhere. The main Li-bearing minerals of the Battonya Complex are biotite and muscovite. Chloritisation and subordinate sericitisation result in significant lithium loss. Chlorite can incorporate Li in its crystal lattice but to a lesser degree than the other sheet silicates, like biotite and muscovite.

1. Introduction

Lithium (Li) has recently become one of the most in-demand elements critical to the global economy as an essential resource for the battery business and, to a lesser extent, for industries such as ceramics and glass production and lubricant grease production. For example, as electric cars become more popular, the global lithium demand (for producing Li-based batteries) is increasing dramatically. Additionally, Li-based batteries will continue to operate in computing products, cell phones, and small household appliances. Furthermore, Li is also used in various other industries (albeit with less usage), such as those producing ceramics, glass, lubricant grease, polymer production, continuous casting, and air treatment. Consequently, much research on its mining viability and sustainability is underway worldwide. Whether Li will be mined in the future by conventional deep cultivation, salt distillation, or by some alternative technology, such as in situ leaching (ISL) and separation from geothermal wells or seawater, will be determined by geopolitical and economic considerations (Bradley et al., 2017).

Existing literature and industry standards separate Li resources from their economic potential into three types: brines, pegmatite deposits, and battery recycling (Kesler et al., 2012; Vikström et al., 2013). Lithium brines related to salt evaporation lie on the surface between dry basins

* Corresponding author.
E-mail addresses: jancsek@geo.u-szeged.hu (K. Jancsek), janovszkyp@gmail.com (P. Janovszky), galbx@chem.u-szeged.hu (G. Galbács), mtoth@geo.u-szeged.hu (T.M. Tóth).

https://doi.org/10.1016/j.apgeochem.2023.105570
Received 21 June 2022; Received in revised form 26 September 2022; Accepted 11 January 2023
Available online 15 January 2023
0883-2927/

surrounded by mountain ranges at high altitudes. These sites, called "salars" under their local name, can be found in the Andes and on the Tibetan Plateau in China. Argentina, Bolivia, and Chile constitute (Grosjean et al., 2012) and hold 50–60% of the aggregate global Li resources lithium triangle combined (USGS report, 2019, 2020). China also has significant Li resources, but recently, Chinese production has been on a downward trend.

Besides brines, granitic pegmatites are the second most essential Li resources (USGS report, 2020). Australia is the leading pegmatite ore producer and is currently the largest Li supplier to the Chinese economy. In Europe, the following countries (listed in descending order) represent the highest Li production: Germany, the Czech Republic, Serbia, Spain, Portugal, Finland, and Austria (USGS report, 2020).

Pegmatites are coarse-grained igneous rocks of granitic composition formed as zoned dykes or anisotropic-textured intrusives (London, 2018). They are crucial natural sources of various rare elements and are thus primarily classified based on their enrichment tendencies regarding these elements. Černý, 1991 created the classification system that is currently applied and that distinguishes the niobium-yttrium-fluorine-enriched (NYF-type) and Li-cesium-tantalum-enriched (LCT-type) pegmatite, petrogenetic families, as endmembers (Černý and Ercit, 2005). The LCT-type family has a compositional affinity with S-type granites formed in orogenic hinterlands because of extreme granitic fractionation (Martin and De Vito, 2005; Černý et al., 2012; Deveaud et al., 2015; London, 2018). Granite pegmatites, particularly the LCT-type, are the primary source rocks of Li-bearing minerals (Chappell and White, 2001; Bradley et al., 2017). The Li-enriched minerals in granites and granite pegmatites are possible sources of elevated Li in associated groundwater and geothermal water. For example, hydrothermal processes, such as the chloritisation of biotite and the seriticisation of feldspar, may release Li from the altered minerals. Chloritisation is a general and essential hydrothermal alteration process in granites (Wilkinson et al., 2015; Srivastava et al., 2018). The reaction biotite + plagioclase → chlorite + epidote + titanite + muscovite (Eggleton and Banfield, 1985) describes the primary alteration mechanism.

The crystalline basement of the Pannonian Basin in southeast Hungary was first studied in the 1940s–50s (Kovács, 1965). After a seismic survey, the first well was drilled in 1959, followed by numerous hydrocarbon wells (Kovács, 1965) that penetrated only the basin filling Neogene sedimentary sequences. Since then, fractured crystalline hydrocarbon reservoir studies have been the principal focus of research in the area (Szanyi and Kovács, 2010; Vass et al., 2018; Lemberkovics et al., 2020). Significant hydrocarbon reserves are still being exploited, although nowadays, the geothermal potential of the area is becoming a higher priority (Zilahi-Sebess and Gyuricza, 2013; Boda, 2016; Osvald et al., 2017; Békési et al., 2018). Various unpublished industrial reports on hydrocarbon and water wells in southeast Hungary indicate a significant amount of Li in the produced water, in some cases over 200 mg/l. The reservoir rocks for both the hydrocarbon and aqueous fluids are fractured S-type granites ("Battonya Granite") of the basement (Juhász et al., 2002) and their overlying sediments. After determining the elevated Li and iodine (I) content of the high-temperature (≥100 °C) geothermal water, a detailed study of it as a critical element resource was recommended by the Hungarian Geological Survey (Mathieu, 2018, 2001, 2011).

Siekierka et al. (2018) and Wisniewska et al. (2018) tested different methods for extracting Li from geothermal water in Poland. Experiments have also been conducted in Tibet, which has a high potential for lithium from geothermal waters (Sun et al., 2020). Typically, the results of existing studies revealed that Li concentrations in geothermal waters ranged from 10 to 25 mg/l, which was significantly exceeded by the Li content in the water of the Battonya area. Therefore, from a technical and economic point of view, the question arises whether it is possible to combine geothermal extraction with ISL technology to make lithium production more efficient (Seredkin et al., 2016; Sapsford et al., 2017). Although this alternative mining method is not currently used on Li, experiments are being conducted to make doing so economically viable (Reichel et al., 2017; Vu et al., 2013; Kuang et al., 2018; Guo et al., 2019). It is also the case that countless wells were deepened due to hydrocarbon exploitation over the past decades. It is expected that environmentally friendly extraction methods of metallic elements will continue to be sought. Therefore, it is worth exploring alternative ways to effectively stimulate Li production without contaminating local groundwater.

As part of planning Li extraction in Southeast Hungary, the first step is to delineate the main Li-bearing minerals and their host rocks in the Battonya Complex. Simple granites are generally not at the centre of lithium research but rather those where pegmatitic ore deposits have been detected. However, the buried Battonya granites discussed in this article are worth exploring, even in the absence of ore deposits. The study's main aim is to the potential evaluation sources of the elevated lithium concentrations in groundwater.

2. Geological setting

The Pannonian Basin is located between three large mountain belts: the Alps, the Carpathians, and the Dinarides. Two tectonic mega-units (separated by the Mid-Hungarian Tectonic Zone), the Alps-Carpathian-Pannonian (ALCAPA) and the Tisia-Dacia mega-units, formed by different evolutions, define the basement of the basin (Császár et al., 2013; Kiss et al., 2017). The Tisia-Dacia plate fragment belonged to the European plate before the Cretaceous period (Ustaszewski et al., 2009; Posgay et al., 2011; Kiss, 2016; Kiss et al., 2017). The Tisia-Dacia mega-unit runs from southwest Hungary to the northeast of the country. It can also be followed in Croatia, Serbia, and Romania (Kovács et al., 2000; Haas, 2013). As a result of overthrusting during the Cretaceous period, the Tisia is separated into four nappe systems: the Mecsek, Villány-Bihor, Békés-Codru, and Biharia systems (Császár et al., 2013) from north to south. During the Late Oligocene and Early Miocene periods, the ALCAPA moved eastward and attached to the Tisia-Dacia, forming the present-day basement of the Pannonian Basin (Haas et al., 1999; Posgay et al., 2011).

The Battonya Complex is located in southeast Hungary and belongs structurally to the Békés-Codru Unit of the Tisia-Dacia. It comprises various rock types, including Variscan granites, crystalline schists, amphibolites, gneisses, and migmatites (Szederkényi, 1997; Pál-Molnár et al., 2001; Juhász et al., 2002; Hováth and Maros, 2012). The Battonya–Pusztaföldvár Ridge (Fig. 1), which extends across most of the subunit, separates the two deepest basins of the Pannonian Basin, that is, the Makó Basin in the west and the Békés Basin in the northeast (Hováth and Maros, 2012). These basins are filled with thick Tertiary and Quaternary sediments (Juhász, 1994; Haas et al., 2014). The ridge is approximately 15–25 km long and 10–15 km wide. It has a 1 km subsurface at its highest point and then sinks toward the northeast (Czauner and Mádl-Szőnyi, 2013).

By the Late Miocene period, many of these units were submerged, including the Battonya-Pusztaföldvár Ridge, which reached its current geological state after undergoing a 600-m rise (Haas et al., 1999) before being buried with sediments. The basement is covered by the Békés Conglomerate, lower Miocene in age. The conglomerate zone is generally 30–40 m thick on the slopes but only a couple of meters thick at the top of the Battonya Ridge (Juhász, 1992; Hováth and Maros, 2012). The conglomerate was formed by coastal abrasion and comprises granite pebbles essentially.

Kovács (1965) and Kovács et al. (2000) demonstrated that the Battonya granite intruded during the Variscan period, approximately 340–360 Ma ago. Besides massive granite, some drilling intersected pegmatites. Rhyolites have been described as genetically related to the granites earlier. Still, recent age dating indicated that these units were pyroclastic rocks unrelated to the granites and are approximately 100 million years younger (Szemerédi et al., 2020).

The granites in the Battonya Complex are of a light-grey, greenish-

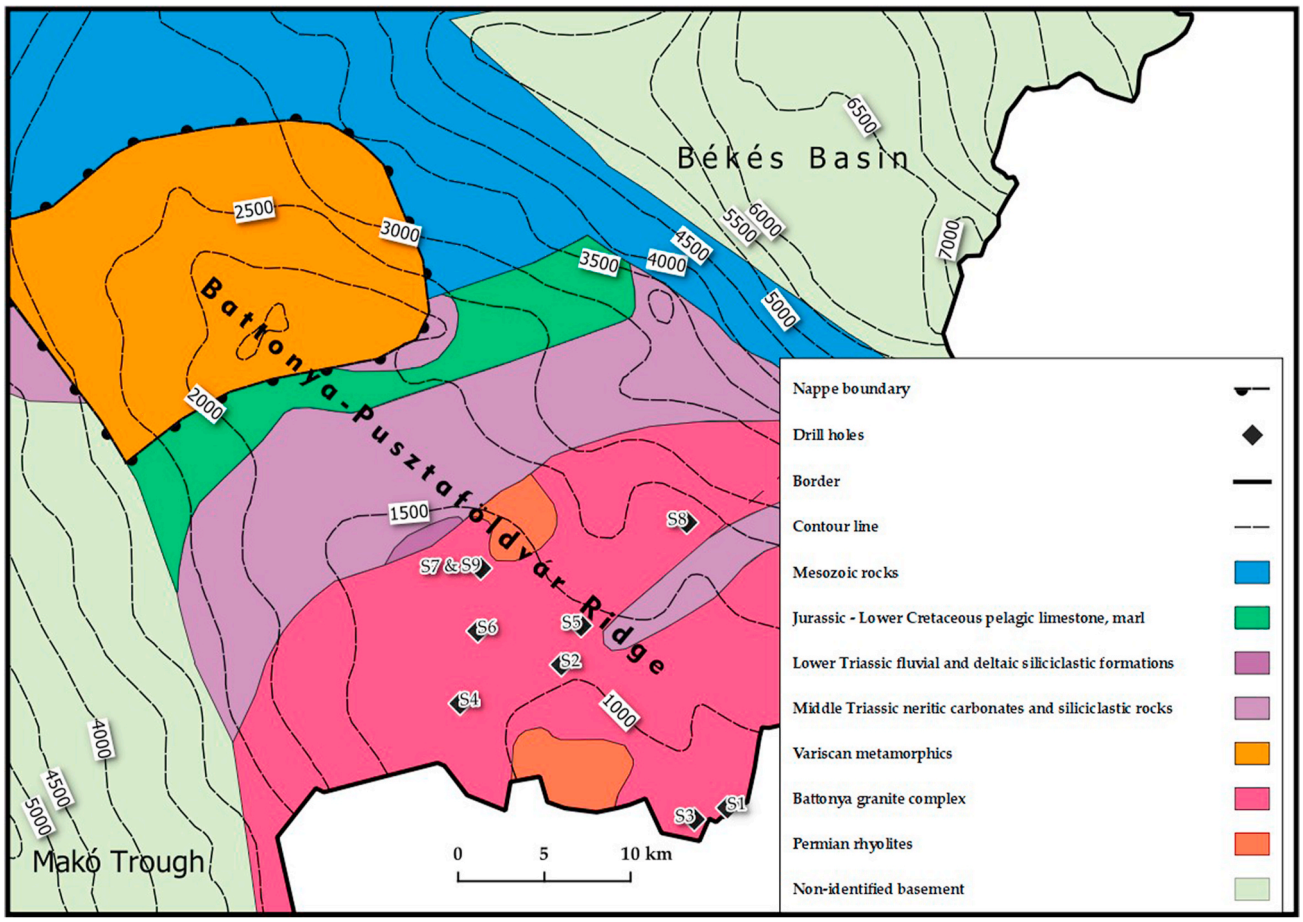

Fig. 1. The location and pre-Cenozoic basement of the Battonya-Pusztaföldvár Ridge. The black dashed contour lines show the basement height below the present surface. The drill-hole locations of the samples used in this study are black diamonds.

grey, and pinkish colour (Szederkényi, 1997; Pál-Molnár et al., 2001; Buda et al., 2012, 2014). Their mineral composition includes quartz, orthoclase, microcline, albite-oligoclase, biotite, and primary and secondary muscovite, as well as apatite, zircon, monazite, and titanite as accessories (Pál-Molnár et al., 2001; Pál-Molnár and Kovács, 2002). Based on the mineral composition, S-type syenogranite, monzogranite, and granodiorite have been distinguished (Pál-Molnár et al., 2001; Pál-Molnár and Kovács, 2002). Their chemical characteristics specify the rock types as granite and granodiorite, with a subalkaline, peraluminous character (Pál-Molnár et al., 2001; Buda and Pál-Molnár, 2012). The rocks are of continental syn-collisional origin. The difference between granodiorite and granite is not explicit, as most samples show various degrees of hydrothermal alteration and autometasomatism (Buda et al., 2012). Apart from these rocks, the massive granite body contains I-type amphibole-bearing quartz monzodiorite mafic enclaves (Buda and Pál-Molnár, 2012). Buda et al. (2012) and Buda and Pál-Molnár (2012) suggested that the granodiorite and granite formed from a low-temperature water-saturated "minimum" peraluminous granite melt at 650–685 °C and pressure above 490 Mpa, indicating that magmatic crystallisation occurred at a depth of approximately 15 km. Chlorite, sericite, epidote, and limonite also occur as secondary phases resulting from various alteration processes. The basic petrographic features of the principal rock types in the Battonya Complex are summarised in Table 1.

3. Materials and methods

Granite and pegmatite specimens were first studied to classify the rock types in the study area petrographically. Finally, nine drill core samples from boreholes representing the Battonya-Pusztaföldvár Ridge (marked S1–S9) were selected to represent the essential macroscopic differences (Table 2.). A crucial parameter in the selection was the level of alteration, with S1 representing the least-altered group of granites and S9 being the most-altered group; S4 was a pegmatite sample with a slight alteration.

Table 1
A summary of the main granite rock types in the Battonya Complex. The mineral abbreviations follow Whitney and Evans (2010).

Rock-types	Colour	Mineralogy	Al-saturation	Geochemical classification	Alteration
Quartz monzodiorite	greenish grey	Amph-Bt without primary Ms, Mc and Qz uncommon	metaluminous- marginally peraluminous	I-type	Pl sericitisation, Bt chloritisation
Two-mica granodiorite – granite	grey	Bt-Ms, Ms alone or subordinary Mc megacrystal, Qz prevalent	peraluminous	S-type	Plg sericitisation, Bt chloritisation

Table 2
Borehole samples marked from S1 to S9 in this study and their macroscopic attributes. The order of the samples is based on the macroscopic and microscopic differences found later.

Drill holes	Depth (m)	Macroscopic attributes
S1	1079–1082	- medium-to-coarse-grained - minerals are easy to distinguish - dark brown biotites - sericitized feldspar
S2	1350–1352	- medium-to-coarse-grained - minerals are easy to distinguish - contiguous biotite layer
S3	1083–1085	- medium-to-coarse-grained - similar to S1, but some greener parts indicate chlorite
S4	1235–1237.5	- coarser-grained - muscovite and chlorite are easy to identify - simple mineralogy
S5	1328–1330	- medium-to-coarse-grained
S6	1191–1195	- greenish colour due to chloritisation - sericitisation
S7	1287.5–1290.5	- medium-to-coarse-grained
S8	1797–1804	- similar appearance
S9	1287.5–1290.5	- biotite and chlorite are absent - some large muscovite flakes - weathered, dusty feldspar due to intensive sericitisation

3.1. Whole-rock geochemistry

Major and trace element compositions in whole-rock samples, including Li concentrations, were analysed with 15 g of rock powders obtained from drill cores using inductively coupled plasma atomic emission spectrometry (ICP-AES) at the Institute of Chemistry of the University of Miskolc, Hungary. For the measurement, the Varian 720 ES, a simultaneous, multi-element ICP-AES spectrometer with an axial plasma view, was used. Certipur (Merck Ltd.) and Spectrascan (Teknolab) solutions were applied as reference materials. The required amount of material for one measurement was 0.2 g. The sample material was placed into a platinum crucible, and 2 mL hydrofluoric acid and 0.75 mL perchloric acid were added. Each sample was gently heated on a hot plate, and 2 cm^3 perchloric acid, 3 cm^3 hydrochloric acid, and 3 cm^3 distilled water were added to the residue. Then, the mixture was heated until it had entirely dissolved in the acid mixture. After cooling to room temperature, the sample was transferred into a 50-cm^3 volumetric flask. The flask was filled up to the mark with distilled water and shaken. Finally, the solution was filtered through a medium-fast paper filter. A blank solution mixture of perchloric and hydrochloric acid with the same concentration was also prepared.

3.2. Laser-induced breakdown spectroscopy

Measuring Li with LIBS is a relatively new approach (Sweetapple and Tassios, 2015). Previously it was mainly detected by LA-ICP-MS and ion microprobe. Although the three instruments are fundamentally similar, modern microprobes are complicated and expensive, whereas LA-ICP-MS is more energy-intensive, needs sample preparation and has no portable version. In contrast, LIBS can be used successfully for laboratory and on-site measurements from unprepared samples of any physical state (Harmon et al., 2013; El Haddad et al., 2014; Galbács, 2015). Consequently, LIBS is increasingly used in geochemical research, particularly for detecting light elements, such as Li (Sweetapple and Tassios, 2015; Fabre et al., 2021; Wise et al., 2022). In previous work, the authors used it successfully to study granites and their Be and Li content (Janovszky et al., 2021). For this study, Li concentrations needed to be measured without sample preparation owing to the limited availability of drill cores from the sub-surface of the Battonya area.

The Li concentration of individual rock-forming minerals from each granites sample was measured using laser-induced breakdown spectroscopy (LIBS) at the Department of Inorganic and Analytical Chemistry, University of Szeged, Hungary, using an Applied Spectra J-200 tandem laser ablation (LA)/LIBS spectrometer. The measurements were carried out on polished rock sections (~100 μm thickness). For measurement sensitivity, a large beam diameter of 40 μm was used, and relatively large grains reasonably homogeneous based on the camera image of the spectrometer were selected for analysis. At least five grains were measured from each mineral type in each sample. Thus a total of 180 data points concerning the Li concentration were analysed. Alkali and plagioclase feldspar grains were not distinguished. They were not considered the primary target species for the research, and similar Li concentration values were expected based on existing research. The laser operation parameters were as follows: 16 mJ pulse energy; 40 μm laser focal spot diameter; 10 repetitions in one spot; 10 Hz laser pulse repetition frequency; 0.5 μs and 1.05 ms spectral data collection gate delay and width, respectively; and 1 l/min argon gas flow rate. Additionally, NIST 610, NIST 612, and NIST 614 glass and the JF-1 feldspar and CRPG Biotite Mica Fe standards were used for quantitative calibration. Plasma emission was detected at the Li 670.78 nm spectral line. The lower detection limit was approximately 1 ppm of Li.

4. Results

4.1. Petrology and the alteration series

The nine drillcore samples are shown in Fig. 2. Concerning their texture, all the granite samples were medium-to-coarse-grained, with large (up to 10–20 mm) idiomorphic K-feldspar crystals. The main rock-forming minerals of all the samples were identical: quartz, feldspar, and subordinate biotite and muscovite. Chlorite typically forms pseudomorph substituting biotite. Accessory minerals, such as apatite, zircon, monazite, and titanite, are of magmatic origin, whereas epidote and carbonate minerals are essential hydrothermal alteration products. Veins of different mineral infill (quartz or siderite) frequently crosscut the samples. Two main alteration processes, sericitisation of feldspar and chloritisation of biotite, were used to define the alteration groups.

The pegmatite sample (S4) was coarser-grained, quartz-rich, and contained alkali feldspars, including microcline. The few muscovite and chlorite flakes typically adjoin each other. The sample was visually similar to the leucogranites based on the abundance of quartz and feldspars and the lack of many mafic grains. Its sericitisation was less advanced.

Based on the level of sericitisation and chloritisation, an approximate alteration series was defined for the granodiorite-granite samples studied from S1 to S9. This series was later simplified to include four groups (*Degree of alteration* 1–4) based on the degree of alteration (Fig. 3).

Degree of alteration 1. Samples S1 and S2 samples belong to this group, with the difference compared with the other samples being the presence of biotite. In most cases, these grains were unaltered or weakly chloritized, and the intensive pleochroism of biotite flakes was observed. The S1 biotite grains were brownish, whereas those in S2 were greenish brown, suggesting lower titanium oxide levels and a nearly equal proportion of iron and magnesium in the minerals. Large muscovite flakes were usually present next to the biotite, suggestive of magmatic origin.

In contrast, the intergranular, thin muscovite flakes were likely the result of post-magmatic processes (Buda et al., 2012). Furthermore, subordinate sericitisation of feldspar occurred in the samples.

Degree of alteration 2. The S3 granite and S4 pegmatite samples belong to this alteration type. In these samples, the replacement of biotite with chlorite was common, although the original texture could still be identified. The sericitisation was not advanced. Sample S3 was less coarse-grained and contained more mafic mineral grains. The

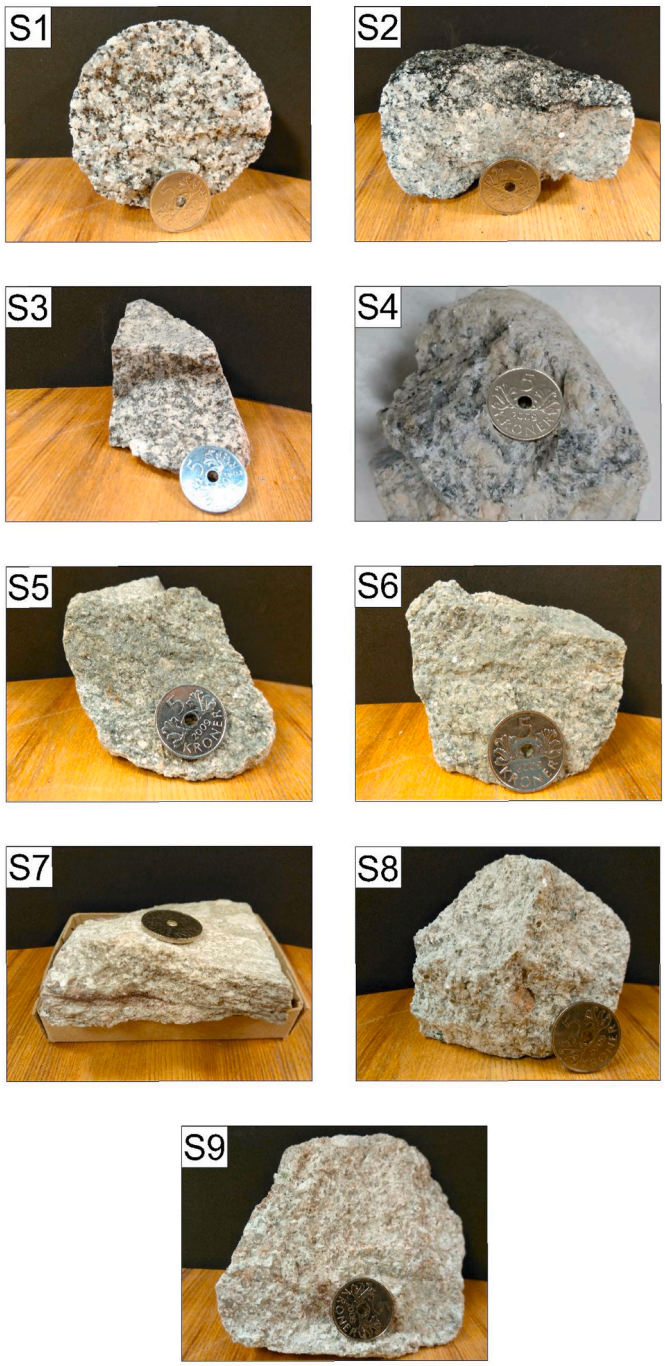

Fig. 2. Drillcore samples S1–S9. Pegmatite is marked as S4, and the coin shown for scale is 2.6 cm in diameter. Samples S1–S3 include dark brown biotite in various concentrations, whereas chloritisation occurred in samples S4 to S6. Samples S7–S9 were more leucocratic and comprised mainly muscovite as the main mica species.

subordinate chloritisation of biotite was observed here, and several residual biotite plates were observable between the chlorite plates. The primary muscovite was reasonably intact and often occurred around the chlorite flakes.

Degree of alteration 3. The granite samples S5 and S6 were part of the third group. In these samples, enhanced alteration caused the pseudomorphic substitution of biotite by chlorite, while the rate of sericitisation was greater. The light- and dark-green chlorite flakes exhibited lavender-brown interference colours. In addition, an aggregate of fine-grained rod-shaped chlorite grains appeared along the vein edges.

Degree of alteration 4. Samples S7–S9 were part of the most-altered group of granites. Veins and cracks filled with sericite and, less frequently, carbonate species characterise the most altered samples. Feldspar sericitisation controlled by veins and microcracks appeared advanced, although alkali feldspar was more resistant to alteration than plagioclase. Muscovite was almost the only primary mica, suggesting that the samples of this group were muscovite-bearing granites. Thin siderite veins also crosscut S9.

4.2. Major and trace element composition

The major element compositions of the samples are shown in Table 3. The rock samples studied are generally similar in composition, except for the S4 pegmatite. The most different features of the latter are the high silica and low aluminium concentrations. There is more significant variation in the CaO, Na_2O and K_2O content of granites. The trace element compositions relevant to this research are presented in Table 4. The indicated trace element concentrations were generally similar in the samples. As can be seen, the total Li content of the whole-rock samples ranged from 1 to 36 ppm.

4.3. Lithium content of the rock-forming minerals

Quartz, feldspar, and muscovite were present in all the samples, thus providing a complete data set, in contrast to biotite and chlorite, which could be identified only in certain samples. The points to be analysed were selected based on the LIBS camera image. A total of 274 points were measured, and ten spectra were taken for each point. Altogether 20 biotite, 78 muscovite, 34 chlorite, 68 feldspar and 74 quartz grains were analysed. Although quartz was the second most abundant mineral measured, only four samples, S1, S2, S4 and S7, provided lithium data due to low intensity. In the other cases, the measured Li data from quartz were invaluable. All the measured Li values are presented in Table 5. As a general assumption, the Li data vary in a wide range, and the following trend can be observed: biotite > muscovite > chlorite > feldspar > quartz.

5. Discussion

5.1. Relationship between alteration state and lithium content

To hypothetically specify the origin of the elevated Li concentration in the groundwater along the southeastern Great Plain in Hungary, the essential priority was identifying the possible source rocks and their petrology, mineralogy, and chemistry. Comparing the results from the microscopic analysis with those of previous studies, a correlation was observed with the rock types determined by Pál-Molnár et al. (2001), Pál-Molnár and Kovács (2002), and Buda et al. (2012). In the samples studied, amphibole was absent. Accordingly, the type-I quartz-monzodiorite was excluded from this paper. As a result, the samples studied corresponded to the usual granodiorite-granite group (types II–III) with two-mica or a solely muscovite form.

The major element diagrams (Fig. 4) revealed that although CaO decreased and K_2O increased with intensifying alteration, the Na_2O concentration was independent of the post-magmatic processes. These observations indicated that intensive sericitisation affected the plagioclase, preferably causing K-gain in the rock body. The Ca^{2+} was likely released into the water, as Mathieu (2018) demonstrated in summary about different hydrothermal alteration mechanisms, including sericitisation of feldspars. The TiO_2, FeO_{tot}, MnO, and MgO contents decreased along with the alteration trend. This combined effect was probably related to the chloritisation of biotite.

The S4 pegmatite contained negligible concentrations of major oxides besides silica and alkalies, agreeing with the microscopic findings.

The diagrams for selected trace elements (Fig. 4) exhibited similar geochemical characteristics, resulting in similar trends. The Li content

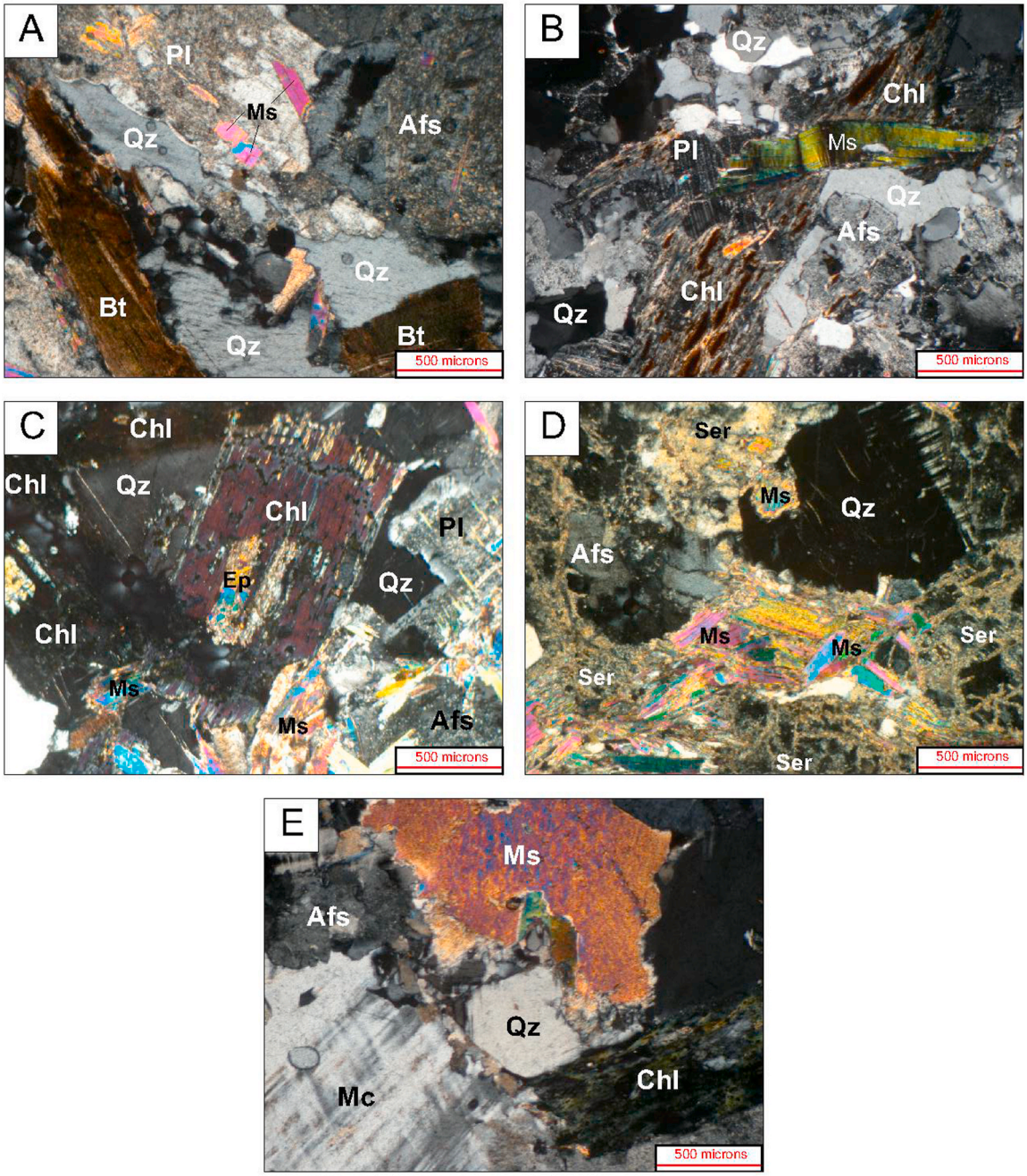

Fig. 3. Photomicrographs of examples of the alteration series as defined by mineralogical characteristics. (A) *Degree of alteration 1*: Intact biotite flakes, weak sericitisation of feldspars, muscovite flakes, and subhedral quartz grains. (B) *Degree of alteration 2*: Biotite, almost altered to chlorite with remnants of biotite. (C) *Degree of alteration 3*: Typically contains chlorite with epidote infill, sericitized feldspars, and small muscovite flakes. (D) *Degree of alteration 4*: Characterised by the extensive sericitisation of feldspars along veins and the occurrence of secondary muscovite. (E) The S4 pegmatite sample with muscovite and chlorite is assigned to the second alteration group. Abbreviations: Bt – biotite, Ms – muscovite, Chl – chlorite, Qz – quartz, Ep – epidote, Pl – plagioclase, Afs – alkali feldspar, Mc – microcline.

steadily decreased along with the alteration trend, as did those of the light rare earth elements La, Ce, and Nd. The V trend mimicked that of Ti, whereas the behaviour of Rb was similar to that of K_2O. The extent of the alteration was analysed using the Al – Na + Ca – K diagram (Fig. 5a). The petrographically determined alteration series exhibited a chemically more diverse picture. The samples indicated a trend from increased Na_2O + CaO to more Al_2O_3- and K_2O-rich compositions, as shown in Fig. 4. Five samples are concentrated around the average granite composition. The higher Na_2O + CaO content indicated less-altered plagioclase in the relatively fresh samples. However, S1 and S3 contain less Al_2O_3 than the average granite composition. Of particular note are samples S2 and S8. S2 had a high Li concentration and intact biotite. Still, it was considered the most-altered sample based on the diagram, despite the lack of advanced alterations observed in this granite type. Furthermore, S8 has a similar composition to the less altered S3.

In the chlorite-carbonate-pyrite index – alteration index (CCPI-AI) diagram (Large et al., 2001; Mathieu, 2018), shown in Fig. 5b, all samples are placed between the sericitisation and chloritisation alteration trends. The alteration features, established both microscopically and chemically, are also visible in the diagram. The three least-altered samples (S1–S3) were close to the chloritisation trend, based on their

Table 3
The major element compositions of the nine representative samples. Values are in oxide wt.%.

Samples	SiO_2	TiO_2	Al_2O_3	FeOtot	MnO	MgO	CaO	Na_2O	K_2O	P_2O_5
S1	71.92	0.18	12.68	2.16	0.04	1.06	0.99	4.38	3.43	0.20
S2	75.37	0.21	15.49	1.38	0.04	0.60	1.71	0.69	1.88	0.29
S3	71.98	0.23	11.70	1.79	0.07	1.56	3.04	2.51	2.43	0.23
S4	87.47	0.05	3.55	0.30	0.01	0.17	0.10	2.29	4.66	0.08
S5	71.44	0.21	15.30	1.29	0.03	0.99	0.50	2.74	4.73	0.30
S6	76.28	0.09	12.83	0.78	0.03	0.70	0.36	1.90	4.81	0.29
S7	74.90	0.09	12.72	0.40	0.04	0.36	0.11	2.24	5.06	0.14
S8	71.82	0.07	13.42	1.54	0.01	0.53	0.84	4.39	4.23	0.05
S9	79.02	0.03	10.37	0.68	0.02	0.17	0.35	2.34	4.49	0.28

Table 4
Trace element compositions of the nine representative samples. Values are in ppm.

Samples	Ag	As	B	Ba	Be	Bi	Cd	Ce	Co	Cr	Cu	Dy	Er	Eu	Ga	Gd	Ge	Hf
S1	11	3	20	392	3	1	5	33	23	7	34	1	1	1	15	3	1	<1
S2	<1	1	67	225	5	1	4	23	14	8	14	1	1	1	16	3	1	<1
S3	4	2	53	378	3	1	6	34	17	15	7	1	<1	1	15	3	<1	<1
S4	5	1	59	537	1	1	3	5	24	12	6	1	<1	<1	9	1	2	<1
S5	<1	4	32	528	1	<1	4	35	21	19	85	2	1	1	17	5	1	1
S6	31	5	25	903	1	2	7	20	23	7	13	1	1	<1	12	3	<1	<1
S7	3	9	72	341	3	1	11	16	19	6	7	1	<1	<1	14	2	2	1
S8	<1	6	28	266	3	2	5	14	11	8	8	<1	<1	<1	13	2	1	<1
S9	1	1	28	737	1	<1	5	6	15	3	5	1	1	<1	9	2	<1	<1

Samples	Hg	Ho	In	La	Li	Lu	Mo	Nb	Nd	Ni	Pb	Pd	Pr	Rb	Re	S	Sb
S1	<1	<1	<1	19	**36**	1	1	7	17	26	26	4	2	152	0	213	5
S2	<1	<1	<1	12	**19**	1	2	8	12	7	14	3	2	110	0	136	3
S3	1	<1	<1	19	**19**	1	2	12	17	10	13	4	2	96	0	565	4
S4	1	<1	<1	3	**1**	1	1	3	2	7	21	1	1	134	0	141	3
S5	<1	<1	<1	18	**17**	1	2	6	19	9	20	4	7	169	0	140	7
S6	1	<1	<1	13	**6**	1	1	3	11	5	19	1	3	173	0	132	9
S7	<1	<1	3	10	**8**	1	2	6	9	5	22	2	4	216	<1	1372	6
S8	<1	<1	<1	7	**2**	<1	1	7	7	4	120	1	2	222	<1	91	2
S9	1	<1	<1	3	**1**	1	1	5	4	3	17	<1	2	165	<1	187	5

Samples	Sc	Se	Sm	Sn	Sr	Ta	Tb	Th	Tl	Tm	U	V	W	Y	Yb	Zn	Zr
S1	3	6	4	5	236	<1	1	5	<1	<1	5	37	409	6	1	91	10
S2	5	5	3	5	285	1	1	4	<1	1	6	39	233	11	1	77	9
S3	4	2	4	10	212	3	<1	6	1	<1	9	46	128	5	1	82	29
S4	1	7	1	4	134	2	<1	1	<1	1	5	6	458	2	<1	46	7
S5	4	6	5	7	162	<1	1	6	<1	<1	6	39	567	9	<1	59	30
S6	3	7	3	7	191	<1	<1	4	<1	<1	4	23	529	9	1	66	10
S7	3	5	2	3	98	2	<1	4	<1	<1	3	21	360	6	<1	49	17
S8	3	3	2	7	102	<1	<1	2	<1	<1	5	12	213	3	1	160	8
S9	2	4	1	2	113	1	<1	2	<1	<1	5	8	272	7	1	26	7

biotite-chlorite content, whereas more intense chloritisation and sericitisation were featured in the S5 and S6 rock types. Finally, samples S7–S9 were close to the sericitisation trend, consistent with the microscopic observations. Overall, the chemically diverse picture of the Battonya rocks results from two initial alteration processes: sericitisation and chloritisation. These processes were driven by the interaction between the host rocks and the percolating fluids, along with fractures and shear zones (Juhász et al., 2002; Varsányi and Kovács, 2005; Vass et al., 2018). In line with this process, cracks and vein fillings appear in the samples of alteration groups 3 and 4.

Regarding the Li content of the Battonya rocks and considering that the average Li concentration in the Earth's crust is approximately 20 ppm (Lide, 2004; White, 2013), only sample S1 sample with 36 ppm of Li could be viewed as a slightly Li-enriched granite. The remaining samples generally exhibited decreased Li content from the average granite composition. The relationships between Li and the major elements are shown in Fig. 6. Positive covariations were observed between Li, MgO and FeO. This can be explained based on the more significant amount of biotite and/or chlorite in the samples. There was also a positive correlation between Li and Al2O3, along with two trends indicating an Al loss occurred during chloritisation and sericitisation. Based on their K2O content, the samples were divided into two groups: one with high K2O and low Li and another with the opposite trends, indicating that the coeval K-gain and Li loss were caused by sericitisation. As CaO decreased, the Li content declined slightly, caused probably by plagioclase alteration.

5.2. Lithium content of different granites

Research on the Li content of granites and their associated pegmatites began in the past century and has become increasingly important with the demand for Li today. In this context, rare earth element-rich granites, particularly LCT-type pegmatites, have been reported as the main lithium-bearing rock types in the literature. As these rocks are formed by advanced or extreme fractionation, they usually contain exotic Li-rich minerals, such as spodumene, lepidolite, and zinnwaldite. Thus, they typically have Li concentrations higher than conventional granites (Maneta and Baker, 2019). However, pegmatites alone are not necessarily associated with a high Li content. For example, in the Sparrow pluton, the spodumene-bearing pegmatites further from the centre of the granite assemblage contain more Li.

For the samples examined, the Li content of the relatively fresh Battonya granites (S1, S2, S3) is indifferent. In comparison, the S-type medium-pressure granites and granodiorites of the Irish Leinster Granite

Table 5
The measured average Li concentrations in different minerals from LIBS analysis. Values are in ppm. Abbreviations: a – average, **σ** – standard deviation, min – minimum, max – maximum, n – number of repetitions, * –intensities below the detection limit. Values are in ppm.

Sample	S1					S2					S3				
	a	σ	min	max	n	a	σ	min	max	n	a	σ	min	max	n
Quartz	17	21	1	81	100	6	7	1	38	100	*	*	*	*	100
Feldspar	88	57	21	243	100	34	14	15	80	100	141	61	74	265	100
Muscovite	1944	338	1320	2970	80	1171	257	876	1990	80	1474	423	951	2977	120
Chlorite	–	–	–	–	–	–	–	–	–	–	2520	399	1645	3298	100
Biotite	3789	511	2260	5149	100	2236	467	1023	3076	100	–	–	–	–	–
Sample	**S4**					**S5**					**S6**				
	a	**σ**	**min**	**max**	**n**	**a**	**σ**	**min**	**max**	**n**	**a**	**σ**	**min**	**max**	**n**
Quartz	2	1	1	6	140	*	*	*	*	50	*	*	*	*	50
Feldspar	17	22	3	93	80	32	12	5	49	50	22	17	4.5	75	50
Muscovite	593	275	169	1571	190	715	132	537	1022	50	511	205	98	833	50
Chlorite	1081	229	365	1600	140	467	72	355	675	50	252	167	21	534	50
Biotite	–	–	–	–	–	–	–	–	–	–	–	–	–	–	–
Sample	**S7**					**S8**					**S9**				
	a	**σ**	**min**	**max**	**n**	**a**	**σ**	**min**	**max**	**n**	**a**	**σ**	**min**	**max**	**n**
Quartz	4	3	1	9	50	*	*	*	*	80	*	*	*	*	50
Feldspar	32	5	21	46	50	68	53	0.4	189	100	26	9	8	43	50
Muscovite	201	76	109	399	50	148	48	83	296	100	150	65	60	364	50
Chlorite	–	–	–	–	–	–	–	–	–	–	–	–	–	–	–
Biotite	–	–	–	–	–	–	–	–	–	–	–	–	–	–	–

batholite contain an average of 275 ppm Li (O'Connor et al., 1991), which is twice as high as the concentrations measured in the Battonya rocks. The Variscan peraluminous porphyritic granite pluton and microgranite of the La Pedriza pluton in the Spanish Central System contain 30.8, 32.2, and 19.5 ppm Li (Pérez-Soba and Villaseca, 2019), making them comparable to the fresh Battonya samples. In the studied case, the post-magmatic alteration of the granites is suggested to have led to Li release, as reflected in the elevated Li concentrations in the geothermal waters surrounding the Battonya area. Similarly, Simons et al. (2017) attributed the hydrothermal activity to the depletion of Li in tourmaline granites studied. Table 6 summarises the Li content of different S-type peraluminous granites from the literature.

5.3. Li concentration of the granitoid minerals

Based on the LIBS measurement results, the following order was established regarding the Li content of the minerals studied: biotite > muscovite > chlorite > feldspar > quartz. Considering the measured data, Fig. 7 shows the lithium content of the rock-forming minerals as a function of alteration groups. Biotite and muscovite were the main Li-bearing minerals in the first alteration group. Both contained two or three orders of magnitude more Li than feldspar and quartz. In the case of sample S3, in which chloritisation was effective, but the original biotite flakes were still observed, the chlorite had higher average Li concentrations than the biotite in sample S2. Subsequently, a similar decrease in concentration was observed for both chlorite and muscovite from approximately 1000 ppm down to a couple of hundred ppm as the alteration evolved. In contrast, the Li concentration in feldspar and quartz retained their Li content due to a lack of alteration. The quartz and feldspar of the intact granites contained slightly more Li than the more-altered ones. In summary, the Li content of the samples decreased as chloritisation and sericitisation progressed. A more detailed analysis of the lithium content of each mineral is presented in the following subsections.

5.3.1. Micas

Among the lithium-containing mica, the trioctahedral trilithionite-polylithionite (lepidolite) and siderophyllite-polylithionite joints (zinnwaldite) are the most important. In their absence in a more common S-type granite, biotite, muscovite, and tourmaline are the main Li-bearing minerals (Hezel et al., 2011; Chakraborty and Upadhyay, 2020). Based on calculations by Bea et al. (1994) and Icenhower and London (1995), Li is compatible in biotite and closer to being incompatible in muscovite (D^{Li}_{Bt}/melt = 1.01–1.67 and D^{Li}_{Mus}/melt = ~0.8). Icenhower and London (1995) also performed the above calculations on peraluminous granite geochemically similar to the Battonya granites. The least altered samples S1 and S2 contain intact biotite and muscovite. The average lithium content of biotite from these two samples is 3789 and 2236 ppm, but the concentration varies over a wide range. The S1 biotite has a minimum value of 2260 ppm and a maximum value of 5149 ppm. Li content in S2 biotite also shows a difference of ~2000 ppm between the two extreme values. For the lithium content of muscovites in the two samples, S1 has a mean of 1944 (min.: 1320, max: 2970), and S2 has a mean of 1171 (min.: 876, max. 1990 ppm). For comparison, in several granite types of the Cornubian batholith, the biotite variety siderophyllite contains a relatively wide range of Li (2000–6000 ppm), whereas the muscovite varies between 1250–3000 ppm. Konings et al. (1988) also analysed mica with high Li concentrations. They found that in Abas granite, metasomatism resulted in biotite with a Li content of approximately 3000–6000 ppm, whereas less-overprinted micas had a Li content of roughly 1000–2000 ppm. The chloritisation of biotite will be discussed in more detail in the following subsection.

Fig. 7 shows that the lithium content of muscovite gradually decreases as the alteration progresses, from an initial value above 1000 ppm to 100–200 ppm in the most altered S7, S8 and S9 samples. The lowest lithium content of 60 ppm was measured in the latter one. Kretz et al. (1989) detected Li at a mean concentration of 120 ppm in two-mica granites from the Sparrow pluton. In contrast, Li was detected at concentrations of 3700 ppm in some biotite grains that had been partially replaced by chlorite and approximately 1000 ppm in muscovite. Concurrently, the Li-mica varieties zinnwaldite and lepidolite include 16,000 and 22,000 ppm Li, respectively (Simons et al., 2017). As an example of the increase in Li content with fractionation, Li concentrations of 200–500 ppm have been measured in the fertile granites of the Superior pegmatite field in Canada, which generated rare earth element-rich pegmatite dikes. Here, the concentrations were 500–2000 ppm in the beryl-type pegmatites and above 2000 ppm in the spodumene subtype in muscovite (Selway et al., 2005). Furthermore, the Cs and Rb content of Fe-rich muscovite and biotite increased in parallel with alterations. These Li concentration values of a couple of thousand ppm were similar to those measured in the S1 sample. However, its 36 ppm bulk concentration was significantly lower than the above-mentioned granites. In the case of the Battonya granites, the Li content of the mica decreases with the progress of chloritisation and sericitisation.

As the primary Li containers in granites are biotite and muscovite,

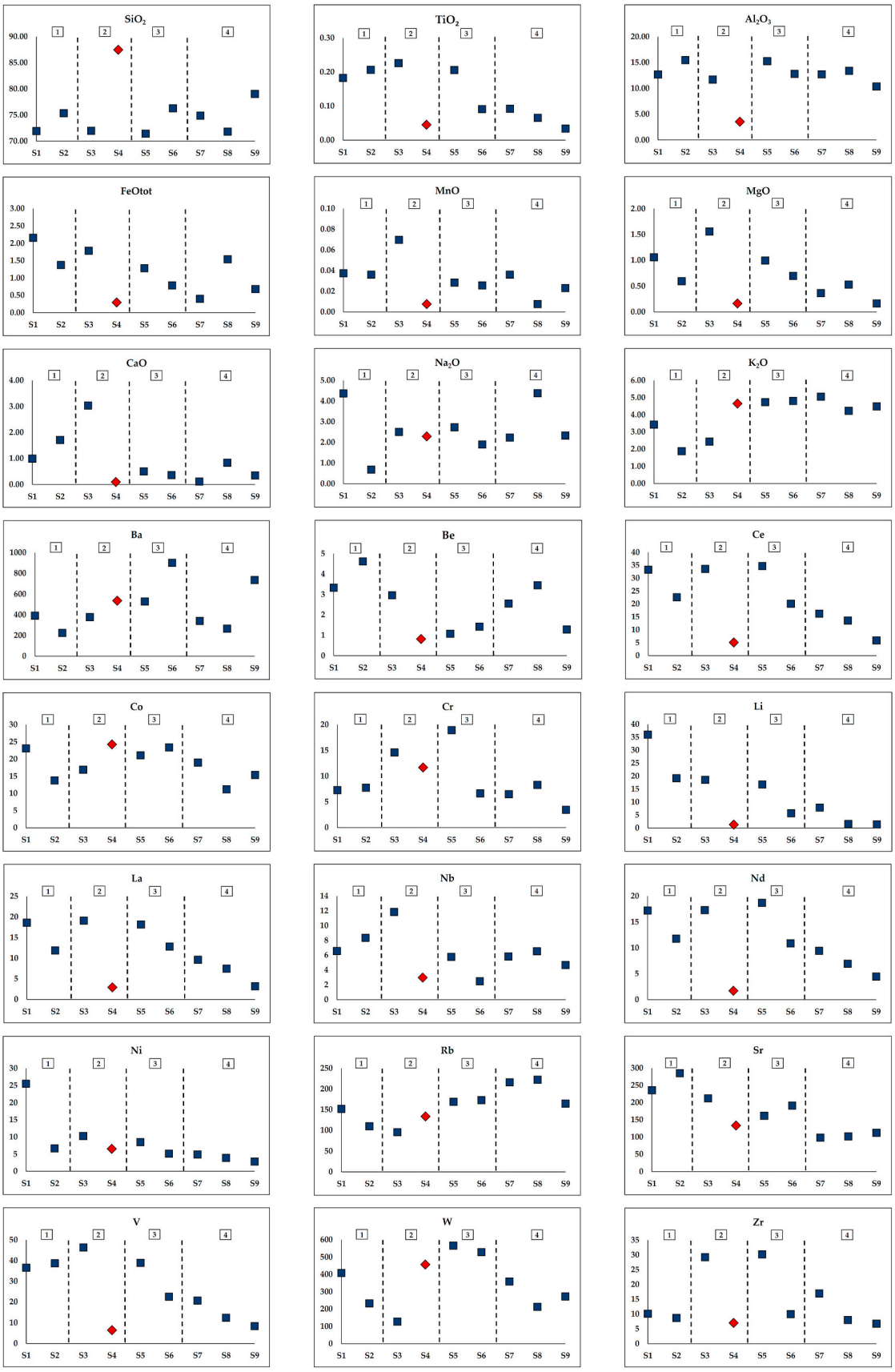

Fig. 4. Major oxide (wt% oxide) and trace element (ppm) diagrams as a function of the interpreted alteration series. The granites are marked as dark-blue squares and the pegmatite as a red diamond.

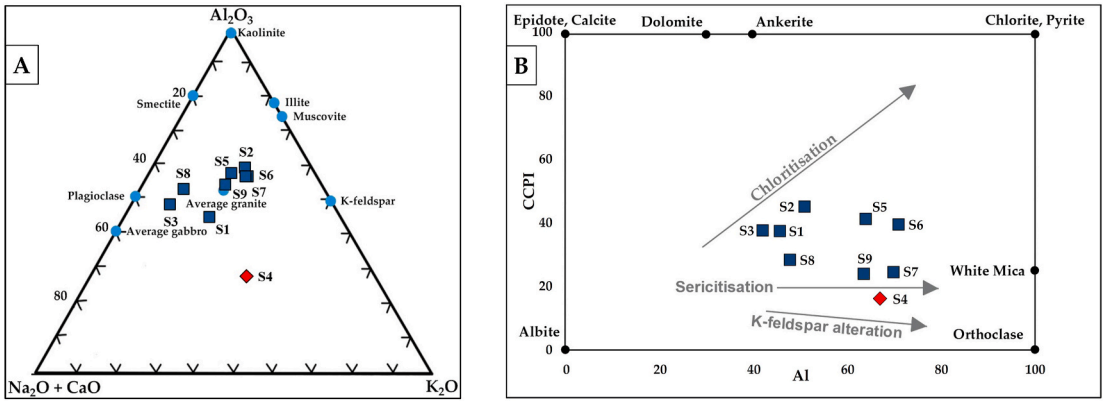

Fig. 5. (a) The Al – Na + Ca – K granite alteration diagram, following Nesbitt and Young (1984, 1989) and Kanamaru et al. (2018). (b) A modified chlorite-carbonate-pyrite-index (CCPI) versus alteration index (AI) alteration box plot, following Large et al. (2001) and Mathieu (2018). For legend, see Fig. 4.

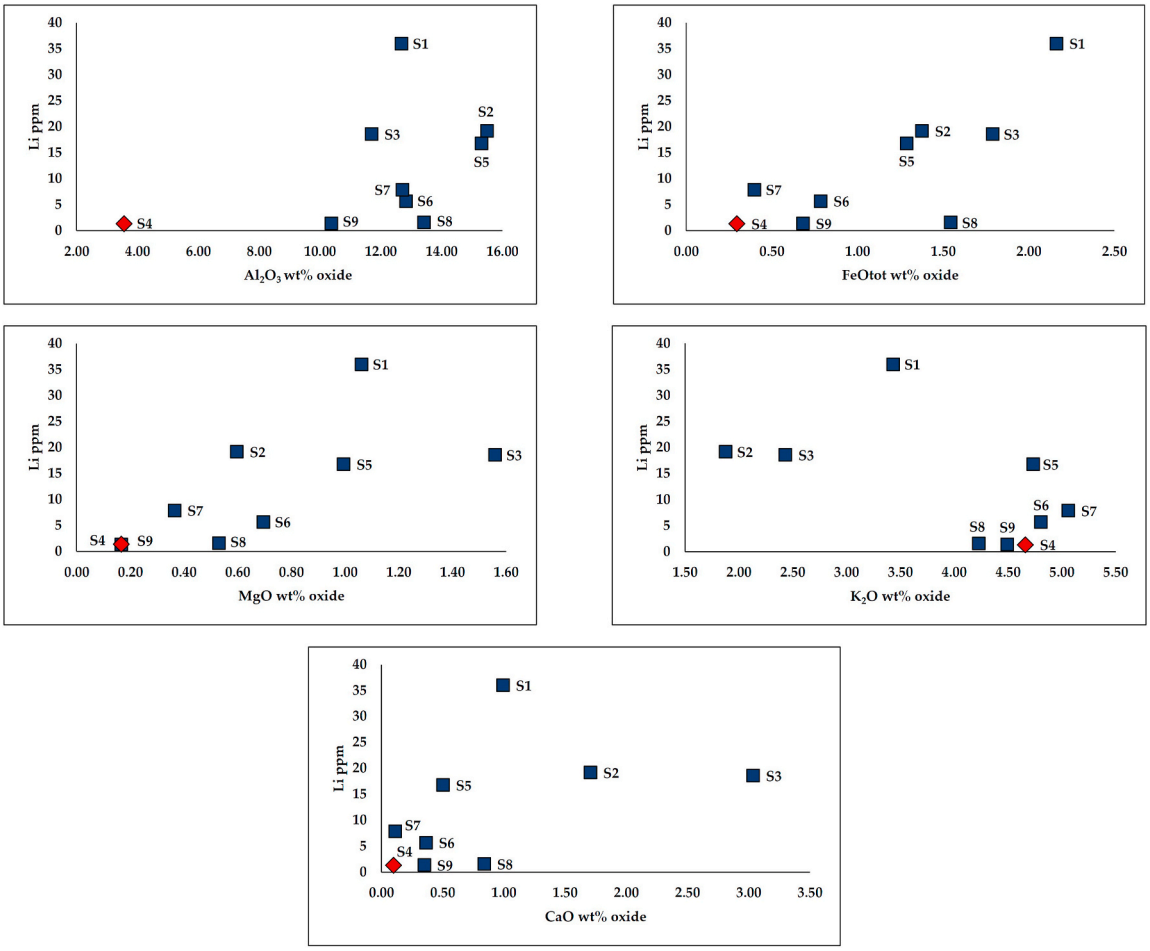

Fig. 6. Plots of relations between major elements and Li. For legend, see Fig. 4.

the bulk Li content depends on the proportion of micas, as demonstrated in Li et al. (2018). Fig. 8 shows a comparative diagram of the measured and previously published whole rock, biotite, and muscovite data. Similar to the data from the literature, the micas in this study contained the most Li in samples with the highest bulk Li content. Moreover, the Li content of the Battonya micas was within the range typical for similar granites. Nevertheless, the high Li concentration in the Battonya micas was not associated with a high bulk composition because of the relatively low amount of mica and the total absence of Li minerals in the granites studied.

5.3.2. *Chloritisation*

Generally, the Li concentration of chlorites has not been a significant focus of previous studies (Bobos et al., 2007). Although a Li-rich member of the chlorite group, cookite is naturally occurring. In addition to cookeite, the Al-bearing donbassite chlorite species can have Li in its dioctahedral position (Lopez et al., 1993).

The mechanism acts in a complex system that affects biotite and constantly evolves with the surrounding grains. It was also observed in S3, resulting in secondary minerals, such as epidote, titanite and secondary mica flakes (Neal et al., 2018). Chlorite with tiny amounts of

Table 6
The Li content of different S-type peraluminous granites from the literature.

Authors	Li concentration (ppm)	Rock-type
Luecke (1981)	181	granodiorite
	220	monzogranite
O'Connor et al. (1991)	275	granodiorite/granite
Simons et al. (2017)	108, 252, 290	two-mica monzogranite
	315	muscovite granite
	158, 231	biotite granite
Li et al. (2018)	149	biotite granite
	166	
	38	muscovite granite
	140	
	90	two-mica granite
	209	
Villaros and Pichavant (2019)	55	leucogranite (muscovite scarcity)
	78	
	101	
	710	leucogranite (biotite scarcity)
	95	two-mica granite
	302	
Zhang et al. (2021)	42.2	weathered granite

epidote occurred in sample S5, suggesting the presence of the above process in the study area.

Lithium concentration was measured from the four chlorite-bearing samples, S3, S4, S5 and S6. The highest average concentration was measured in S3 with 2520 ppm, while the minimum and maximum values, in that case, were 1645 and 3298 (Fig. 7). Consequently, the lithium content of the S3 chlorites is higher than the muscovites of the more intact S1–S2 samples and even rivals that of the biotites. The chlorite in pegmatite S4 has less than half the average concentration (1081 ppm) compared to S3, while even more significant decreases were observed in S5 (467 ppm) and S6 (252), which belong to the third alteration group. Thus, there is a 10-fold difference in concentration between the S3 and S6 samples. The high Li concentrations in the chloritized Battonya samples, especially S3, could result from a significant amount of Li being transferred into the chlorite sheets from the precursor biotite. Considering the lower values in S5 and S6, this transformation decreased as chloritisation progressed. Wilkinson et al. (2015) suggested that the variable composition of chlorites indicates that Li substitution is more likely than Li in microinclusions. In the case of Battonya, chloritisation caused Li release, but some of the Li was incorporated into the chlorite during the early alteration stages. Recent research showed that chlorite and the clay mineral montmorillonite might play an important role in sequestering Li released from igneous rocks (Li et al., 2021). For example, at the Naomugeng deposit in China, chlorite contained 1421–2806 ppm Li in surface samples and 2229–3014 ppm in drill cores. The results described in this paper also revealed a high Li content in chlorite, up to approximately 1000 ppm.

5.3.3. Quartz

As expected, quartz contained the least Li among all minerals in the Battonya granites. The intensity values obtained were suitable for concentration calculation for only four samples during LIBS measurement. The highest average concentrations were measured in samples S1 and S2 with 17 and 6 ppm. Although, two outliers, 81 and 36, contributed to these values. They were followed by S7 (4 ppm) and S4 (2 ppm) near the detection limit. Previous research has shown that the incorporation of Li

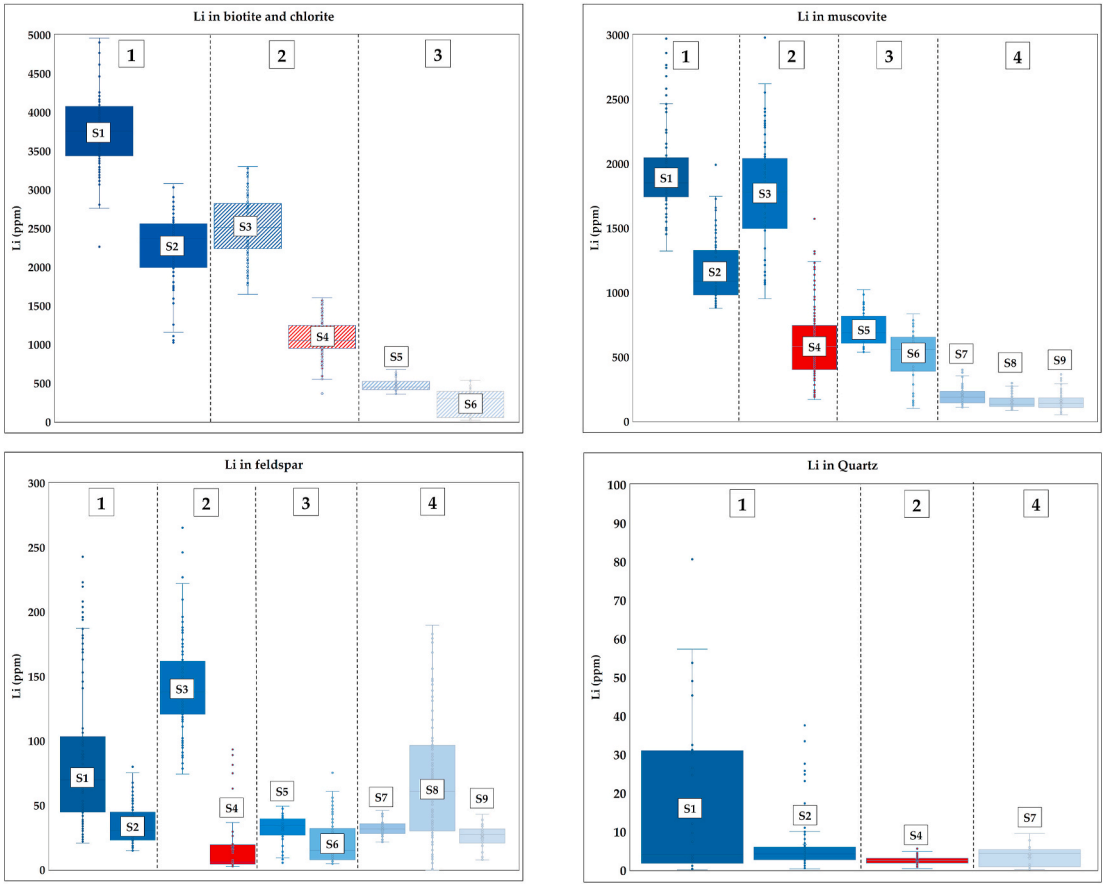

Fig. 7. Box-plot diagrams about the lithium content of the rock-forming minerals as a function of alteration groups. Chlorites are marked as hatched- and S4 pegmatite as red boxes.

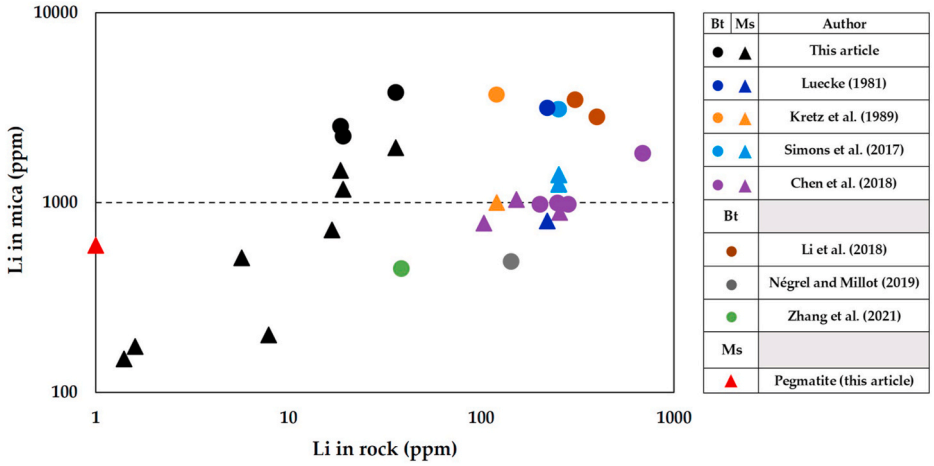

Fig. 8. A comparison of the measured Li concentrations in granites (black symbols), pegmatite (red triangle) and those from previous articles as a function of Li rock and mineral content. Dots and triangles, respectively, represent biotite and muscovite. Data from Luecke (1981), Kretz et al. (1989), Simons et al. (2017), Chen et al. (2018), Li et al. (2018), Négrel and Millot (2019), and Zhang et al. (2021) are presented.

into the quartz structure depends strongly on the amount of Al present in the mineral as alkalies such as Li^+, Na^+, and K^+ have a charge-balancing function during Si^{4+} substitution by Al^{3+}, Fe^{3+}, or B^{3+} (Larsen et al., 2004; Breiter and Müller, 2009). The two possible explanations of Li^+ incorporation into the silica structure in this study are the aforementioned coupled substitution and entering as an interstitial impurity (Götze et al., 2004; Larsen et al., 2004).

Breiter et al. (2013) stated that quartz with a Li concentration over 20 ppm occurred only in strongly fractionated granites. In a later paper by the same authors, highly fractionated S-type rare earth granites contained an average of 40 ppm Li, whereas A-type granites contained only 15 ppm (Breiter et al., 2020). Although quartz grains generally contain Li at a few tens of ppm concentrations, highly fractionated Li-rich pegmatites can contain up to several hundred ppm (Maneta and Baker, 2019). The average measured concentration of the Battonya samples ranged from 4 to 17 ppm. The most plausible explanation for the outlying ppm values of S1 and S2 is microheterogeneity within the grains. Although higher concentrations were found in the less altered group, there is likely no correlation between the lithium content of quartz and the degree of alteration.

5.3.4. *Feldspars*

Similar to quartz, Li is also incompatible with feldspars. Therefore, a low concentration was expected (Maneta et al., 2015). Our samples' average measured Li content varied between 17 and 141 ppm without distinguishing the alkali and plagioclase groups. No substantive change in the Li content of the feldspars was observed as sericitisation progressed. This was also indicated by samples S3 and S8, in which the Li content of the feldspars exceeded or approached that in the less-weathered samples. One possible explanation is that the mica clusters formed during sericitisation incorporated Li, whereas the minerals originally contained more Li in their inclusions, as Smith (1974) suggested. Low values were measured from K-feldspar (4.71 and 8.01 ppm) and plagioclase (0.86, 2.50, and 3.71 ppm) from the Peña Negra Anatectic Complex (Bea et al., 1994). In Portugal, alkali feldspars separated from peraluminous granitic rocks contained a mean of 6 ppm in granites and 15 ppm in aplites and pegmatites, with a 42 ppm maximum (Neiva, 1995). Gordiyenko (1971) and Smeds (1992) believe that feldspars with Li concentrations around 100 ppm could signal the presence of Li aluminosilicate, such as spodumene, in both rare-element granites and pegmatites. In our study, the average values of only three samples were close to this 100 ppm threshold.

6. Conclusion

Overall, chloritisation of biotite and partial sericitisation of feldspar were demonstrated as a potential explanation for the high Li content of the geothermal waters around the Battonya Complex. Formation water in southeast Hungary has a high Li concentration, at approximately 200 mg/l. To determine the source of this Li, nine granite samples were selected from the Battonya Complex for alteration and Li concentration analysis. The microscopic observations and chemical data revealed that the samples had undergone different degrees of hydrothermal alteration from fresh, nearly intact two-mica granites to granites with chloritisation and sericitisation.

Lithium bulk concentrations were determined using ICP-MS, whereas the Li contents of rock-forming minerals, biotite, muscovite, feldspar, and quartz were measured using LIBS. The bulk composition revealed that the least-altered granite samples contained the most Li, comprising intact biotite and primary muscovite. Lithium loss increased with the rate of biotite chloritisation, although chloritized biotite could still trap Li at relatively high concentrations. Furthermore, the Li content decreased as primary muscovite was altered and sericitisation progressed. The Li contents of the minerals were consistent with previous results, following the order biotite > muscovite > chlorite > feldspars > quartz. It should be noted that despite the high concentrations measured in the micas of less-altered granites, the bulk Li content of the rock samples was lower than that reported in previous publications for similar rock types worldwide. This can be explained by the limited amount of micas, especially biotite, in the granite body studied. At present, there is insufficient information on the spatial position, depth, and thickness of different altered granite types. These relationships should be clarified in the future for a detailed economic evaluation.

Declaration of competing interest

The authors declare that they have no known competing financial interests or personal relationships that could have appeared to influence the work reported in this paper.

Data availability

The authors are unable or have chosen not to specify which data has been used.

Acknowledgements

G. Galbács and P. Janovszky gratefully acknowledge the financial support from the National Research, Development and Innovation Office of Hungary under project No. K_129063 and TKP2021-NVA-19.

References

Bea, F., Pereira, M.D., Stroh, A., 1994. Mineral/leucosome trace-element partitioning in a peraluminous migmatite (a laser ablation-ICP-MS study). Chem. Geol. 117, 291–312.
Békési, E., Lenkey, L., Limberger, J., Porkoláb, K., Balázs, A., Bonté, D., Vrijlandt, M., Horváth, F., Cloetingh, S., van Wees, J.D., 2018. Subsurface temperature model of the Hungarian part of the Pannonian Basin. Global Planet. Change 171, 48–64.
Bobos, I., Vieillard, P., Charoy, B., Noronha, F., 2007. Alteration of spodumene to cookeite and its pressure and temperature stability conditions, in Li-bearing aplite-pegmatites from Northern Portugal. Clay Clay Miner. 55 (No. 3), 295–310.
Boda, K., 2016. Fostering geothermal development in Hungary: opportunities and bottlenecks. Unit. Nation Univ.Rep.t 12, 125–168.
Bradley, D.C., Stillings, L.L., Jaskula, W.B., Munk, L.A., McCauley, A.D., 2017. Lithium, chapter K. In: Schulz, K.J., DeYoung Jr., J.H., Seal II, R.R., Bradley, D.C. (Eds.), Critical Mineral Resources of the United States – Economic and Environmental Geology and Prospects for Future Supply. USGS, p. 34.
Breiter, K., Müller, A., 2009. Evolution of rare-metal granitic magmas documented by quartz chemistry. Eur. J. Mineral 21/2, 335–346.
Breiter, K., Ackerman, L., Svojtka, M., Müller, A., 2013. Behavior of trace elements in quartz from plutons of different geochemical signature: a case study from the Bohemian Massif, Czech Republic. Lithos 175–176, 54–67.
Breiter, K., Ďurišová, J., Dosbaba, M., 2020. Chemical signature of quartz from S- and A-type rare-metal granites – a summary. Ore Geol. Rev. 125, 103674.
Buda, Gy, Nagy, G., Pál-Molnár, E., 2014. Allanite and monazite occurrences in variscan granitoids of tisza mega-unit (south Hungary). Carpathian J.Earth Environ. Sci. 9 (No. 1), 57–68.
Buda, Gy, Pál-Molnár, E., 2012. Apatite as a petrogenetic indicator of variscan granitoids in tisza mega-unit (south Hungary). Carpathian J.Earth Environ. Sci. 7 (No. 4), 47–60.
Buda, Gy, Pál-Molnár, E., Koller, F., 2012. Mafic enclaves in peraluminous variscan granitoid in the Battonya unit from southeast Hungary. Geol. Croat. 65/2, 243–253.
Černý, P., 1991. Rare-element granite pegmatites. Part I: anatomy and internal evolution of pegmatite deposits. Part II: regional to global relationships and petrogenesis. Geosci. Can. 18, 49–81.
Černý, P., Ercit, S.T., 2005. The classification of granitic pegmatites revisited. Can. Mineral. 43, 2005–2026.
Černý, P., London, D., Novák, M., 2012. Granitic Pegmatites as reflections of their sources. Elements 8, 289–294.
Chakraborty, T., Upadhyay, D., 2020. The geochemical differentiation of S-type pegmatites: constraints from major–trace element and Li–B isotopic composition of muscovite and tourmaline. Contrib. Mineral. Petrol. 175, 60.
Chappell, B.W., White, A.J.R., 2001. Two contrasting granite types. 25 Years later. Aust. J. Earth Sci. 48, 489–499.
Chen, B., Gu, H-o., Chen, Y., Sun, K., Chen, W., 2018. Lithium isotope behaviour during partial melting of metapelites from the Jiangnan Orogen, South China: implications for the origin of REE tetrad effect of F-rich granite and associated rare-metal mineralisation. Chem. Geol. 483, 372–384.
Császár, G., Szinger, B., Piros, O., 2013. From continental platform towards rifting of the tisza unit in the late triassic to early cretaceous. Geol. Carpathica 64/4, 279–290.
Czauner, B., Mádl-Szőnyi, J., 2013. Regional hydraulic behavior of structural zones and sedimentological heterogeneities in an overpressured sedimentary basin. Mar. Petrol. Geol. 48, 260–274.
Deveaud, S., Millot, R., Villaros, A., 2015. The genesis of LCT–type granitic pegmatites, as illustrated by lithium isotopes in micas. Chem. Geol. 411, 97–111.
Eggleton, R.A., Banfield, J.F., 1985. The alteration of granitic biotite to chlorite. Am. Mineral. 70, 902–910.
El Haddad, J., Canioni, L., Bousquet, B., 2014. Good practices in LIBS analysis: review and advices. In: Spectrochimica Acta Part B: Atomic Spectroscopy, vol. 101. Elsevier, pp. 171–182.
Fabre, C., Qurti, N.E., Mercadier, J., Cardoso-Fernandes, J., Dias, F., Perrotta, M., Koertning, F., Lima, A., Kaestner, F., Koellner, N., Linnen, R., Benn, D., Martins, T., Cauzid, J., 2021. Analyses of Li-rich minerals using handheld LIBS tool. Data 6, 68.
Galbács, G., 2015. A critical review of recent progress in analytical laser-induced breakdown spectroscopy. Anal. Bioanal. Chem. 407, 7537–7562.
Gordiyenko, V.V., 1971. Concentrations of Li, Rb, and Cs in potash feldspar and muscovite as criteria for assessing the rare-metal mineralisation in granite pegmatites. Int. Geol. Rev. 13 (Issue 2), 134–142.
Götze, J., Plötze, M., Graupner, T., Hallbauer, D.K., Bray, C.J., 2004. Trace element incorporation into quartz: a combined study by ICP-MS, electron spin resonance, cathodoluminescence, capillary ion analysis, and gas chromatography. Geochem. Cosmochim. Acta 68 (18), 3741–3759.
Grosjean, C., Miranda, P.H., Perrin, M., Poggi, P., 2012. Assessment of world lithium resources and consequences of their geographic distribution on the expected development of the electric vehicle industry. In: Renewable and Sustainable Energy Reviews, vol. 16. Elsevier, pp. 1735–1744.
Guo, H., Kuang, G., Wan, H., Yang, Y., Yu, H-z, Wang, H-d., 2019. Enhanced acid treatment to extract lithium from lepidolite with a fluorine-based chemical method. Hydrometallurgy 183, 9–19.
Haas, J., Budai, T., Csontos, L., Fodor, L., Konrád, Gy, Koroknai, B., 2014. Geology of the Pre-cenozoic Basement of HungaryExplanatory Notes for "Pre-cenozoic Geological Map of Hungary" (1:500000). Geological and Geophysical Institute of Hungary, Budapest.
Haas, J., 2013. Geology of Hungary. Springer-Verlag, Berlin Heidelberg, p. 246.
Haas, J., Hámor, G., Korpás, L., 1999. Geological setting and tectonic evolution of Hungary. Geol. Hung. Ser. Geol. 24, 179–196.
Harmon, R.S., Russo, R.E., Richard, R.H., 2013. Applications of laser-induced breakdown spectroscopy for geochemical and environmental analysis: a comprehensive review. Spectrochim. Acta B Atom Spectrosc. 87, 11–26.
Hezel, D.C., Kalt, A., Marschall, H.R., Ludwig, T., Meyer, H.-P., 2011. Major-element and li, be compositional evolution of tourmaline in an S-type granite–pegmatite system and its country rocks: an example from Ikaria, Aegean Sea, Greece. Can. Mineral. 49, 321–340.
Hováth, Z., Maros, Gy, 2012. Szegedi-medence Terület Szénhidrogén Koncessziós Jelentése - Komplex Érzékenységi És Terhelhetőségi Vizsgálati Tanulmány - Szeged Basin Hydrocarbon Concession Area: Complex Sensitivity and Resilience Test Study. Magyar Bányászati és Földtani Hivatal (MBFH), Budapest, p. 182.
Icenhower, J., London, D., 1995. An experimental study of element partitioning among biotite, muscovite, and coexisting peraluminous silicic melt at 200 MPa (H_2O). Am. Mineral. 80, 1229–1251.
Janovszky, P., Jancsek, K., Palásti, D.J., Kopniczky, J., Hopp, B., Tóth, T.M., Galbács, G., 2021. Classification of minerals and the assessment of lithium and beryllium content in granitoid rocks by laser-induced breakdown spectroscopy. J. Anal. Atomic Spectrom. 36 (4), 813–823.
Juhász, A., Tóth, M., T, Ramseyer, K., Matter, A., 2002. Connected fluid evolution in fractured crystalline basement and overlying sediments, Pannonian Basin, SE Hungary. Chem. Geol. 182, 91–120.
Juhász, Gy, 1992. A pannóniai (s.l.) formációk térképezése az Alföldön: kiterjedés, fácies és üledékes környezet - Pannonian (s.l.) lithostratigraphic units in the Great Hungarian Plain: distribution, fades and sedimentary environment. Foldtani Kozlony 122/2–4, 133–165.
Juhász, Gy, 1994. Magyarországi neogén medencerészek pannóniai s.l. üledéksorának összehasonlító elemzése - comparison of the sedimentary sequences in Late Neogene subbasins in the Pannonian Basin, Hungary. Foldtani Kozlony 124/4, 341–365.
Kanamaru, T., Suganuma, Y., Oiwane, H., Miura, H., Miura, M., Okuno, J., Hayakawa, H., 2018. The weathering of granitic rocks in a hyper-arid and hypothermal environment: a case study from the Sør-Rondane Mountains, East Antarctica. Geomorphology 317, 62–74.
Kesler, S.E., Gruber, P.W., Medina, P.A., Keoleian, G.A., Everson, M.P., Wallington, T.J., 2012. Global lithium resources: relative importance of pegmatite, brine and other deposits. Ore Geol. Rev. 48, 55–69.
Kiss, J., 2016. A gravitációs és mágneses anomáliák átfogó értelmezése a Kárpát–Pannon-régióban - comprehensive interpretation of gravity and magnetic anomalies in Carpathian-Pannonian Region. Foldtani Kozlony 146/3, 275–298.
Kiss, J., Vértessy, L., Fancsik, T., Kovács, A. Cs, Madarasi, A., Gulyás, Á., 2017. Tisia a geofizikai adatok tükrében és a litoszférakutató szelvények szeizmikusan nagy sebességű zónáinak értelmezése - Tisia – in the light of geophysics and the interpretation of high seismic velocity zones in the crust. Magy. Geofiz. 58, 209–229. évf., 4. szám.
Konings, R.J.D., Boland, J.N., Vriend, S.P., Jansen, B.H., 1988. Chemistry of biotites and muscovites in the Abas granite, northern Portugal. Am. Mineral. 73, 754–765.
Kovács, T.G., 1965. A battonyai terület mélyföldtani felépítése – geology of the Battonya region. Foldtani Kozlony 95/2, 183–189.
Kovács, S., Szederkényi, T., Haas, J., Buda, Gy, Császár, G., Nagymarosy, A., 2000. Tectonostratigraphic terranes and zones juxtaposed along the Mid-Hungarian Line: their contrasting evolution and relationships. Acta Geol. Hung. 43/3, 225–328.
Kretz, R., Loop, J., Hartree, R., 1989. Petrology and Li-Be-B geochemistry of muscovite-biotite granite and associated pegmatite near Yellowknife, Canada. In: Contributions to Mineralogy and Petrology, vol. 102. Springer-Verlag, pp. 174–190.
Kuang, G., Liu, Y., Li, H., Xing, S., Li, F., Guo, H., 2018. Extraction of lithium from β-spodumene using sodium sulfate solution. Hydrometallurgy 177, 49–56.
Large, R.R., Gemmell, J.B., Paulick, H., Huston, D.L., 2001. The alteration boxplot: a simple approach to understanding the relationship between alteration mineralogy and lithogeochemistry associated with volcanic-hosted massive sulfide deposits. Econ. Geol. 96, 957–972.
Larsen, R.B., Henderson, I., Ihlen, P.M., Jacamon, F., 2004. Distribution and petrogenetic behaviour of trace elements in granitic pegmatite quartz from South Norway. Contrib. Mineral. Petrol. 147, 615–628.
Lemberkovics, V., Kiss, K., Váry, M., Kiss, B., Kovács, G., 2020. A jó, a rossz és a csúf? – avagy a szénhidrogén-kutatás dicső múltja, (még) létező jelene és bizonytalan jövője a Pannon-medencében – szemle - The good, the bad and the ugly? – or the past, the (still) existing present and the uncertain future of the hydrocarbon exploration in the Pannonian Basin – Review. Foldtani Kozlony 150/4, 571–610.
Li, J., Huang, X.-L., Wei, G.-J., Liu, Y., Ma, J.-L., Han, L., He, P.-L., 2018. Lithium isotope fractionation during magmatic differentiation and hydrothermal processes in rare-metal granites. Geochem. Cosmochim. Acta 240, 64–79.
Li, C., Li, Z., Wu, T., Luo, Y., Zhao, J., Li, X., 2021. Metallogenic characteristics and formation mechanism of Naomugeng clay-type lithium deposit in central inner Mongolia, China. Minerals 11, 238.
Lide, D.R., 2004. CRC Handbook of Chemistry and Physics, 84th Edition. CRC Press, Florida, USA.
London, D., 2018. Ore-forming processes within granitic pegmatites. Ore Geol. Rev. 101, 349–383.

Lopez, J.M.G., Pérez, I.S., Fernández-Nieto, C., González, I.F., 1993. Lithium-bearing hydrothermal alteration phyllosilicates related to portalet fluorite ore (pyrenees, huesca, Spain). Clay Miner. 28, 275–283.
Luecke, W., 1981. Lithium pegmatites in the leinster granite (southeast Ireland). Chem. Geol. 34, 195–233.
Maneta, V., Baker, D.R., Minarik, W., 2015. Evidence for lithium-aluminosilicate supersaturation of pegmatite-forming melts. Contrib. Mineral. Petrol. 170, 4.
Maneta, V., Baker, D.R., 2019. The potential of lithium in alkali feldspars, quartz, and muscovite as a geochemical indicator in the exploration for lithium-rich granitic pegmatites: a case study from the spodumene-rich Moblan pegmatite. J. Geochem. Explor. 205, 106336.
Martin, R.F., De Vito, C., 2005. The patterns of enrichment in felsic pegmatites ultimately depend on tectonic setting. Can. Mineral. 43, 2027–2048.
Mathieu, L., 2018. Quantifying hydrothermal alteration: a review of methods. Geosciences 8 (7), 245.
Neal, L.C., Wilkinson, J.J., Mason, P.J., Chang, Z., 2018. Spectral characteristics of propylitic alteration minerals as a vectoring tool for porphyry copper deposits. J. Geochem. Explor. 184, 179–198.
Négrel, Ph, Millot, R., 2019. Behaviour of Li isotopes during regolith formation on granite (Massif Central, France): controls on the dissolved load in water, saprolite, soil and sediment. Chem. Geol. 523, 121–132.
Neiva, A.M.R., 1995. Distribution of trace elements in feldspars granitic aplites and pegmatites from Alijó-Sanfins, northern Portugal. Mineral. Mag. 59, 35–45.
Nesbitt, H.W., Young, G.M., 1984. Prediction of some weathering trends of plutonic and volcanic rocks based on thermodynamic and kinetic considerations. Geochem. Cosmochim. Acta 48, 1523–1534.
Nesbitt, H.W., Young, G.M., 1989. Formation and diagenesis of weathering profiles. J. Geol. 97, 129–147.
O'Connor, P.J., Gallagher, V., Kennan, P.S., 1991. Genesis of lithium pegmatites from the Leinster Granite Margin, southeast Ireland: geochemical constraints. Geol. J. 26, 295–305.
Osvald, M., Szanyi, J., Medgyes, T., Kóbor, B., Csanádi, A., 2017. Geothermal energy developments in the district heating of Szeged. Eur. Geol.Eur. Geol. 43, 30–33.
Pál-Molnár, E., Kovács, G., Batki, A., 2001. Petrographical characteristics of variscan granitoids of Battonya unit boreholes (SE Hungary). Acta Minerol.-Petrogr. (Szeged) 42, 21–31.
Pál-Molnár, Kovács, G., 2002. Geochemistry and origin of the Battonya unit granitoids, SE Hungary. Acta Minerol.-Petrogr. (Szeged) 43, 65–69.
Pérez-Soba, C., Villaseca, C., 2019. Li-Na-metasomatism related to I-type granite magmatism: a case study of the highly fractionated La Pedriza pluton (Iberian Variscan belt). Lithos 344, 159–174.
Posgay, K., Bodoky, T., Falus, Gy, Kovács, I.J., Madarasi, A., Gúthy, T., Hegedűs, E., Kovács, A. Cs, 2011. A Tisza és a száva–bükki egység szerkezetének alsó-krétabeli alakulása - structural formation of Tisza and Száva-Bükk units in the Lower Cretaceous period. Magy. Geofiz. 52/3, 135–150.
Reichel, S., Aubel, T., Patzig, A., Janneck, E., Martin, M., 2017. Lithium recovery from lithium-containing micas using sulfur oxidising microorganisms. Miner. Eng. 106, 18–21.
Sapsford, D., Cleall, P., Harbottle, M., 2017. In situ resource recovery from waste repositories. Exploring the potential for mobilisation and capture of metals from anthropogenic ores. Journal of Sustainable Metallurgy 3 (2), 375–392.
Selway, J.B., Breaks, F.W., Tindle, A.G., 2005. A review of rare-element (Li-Cs-Ta) pegmatite exploration techniques for the superior province, Canada, and large worldwide tantalum deposits. Explor. Min. Geol. 14 (Nos. 1–4), 1–30.
Seredkin, M., Zabolotsky, A., Jeffress, G., 2016. In situ recovery, an alternative to conventional methods of mining. Exploration, resource estimation, environmental issues, J. Sustain.Metall.project. Ore Geol. Rev. 79, 500–514.
Siekierka, A., Tomaszewska, B., Bryjak, M., 2018. Lithium capturing from geothermal water by hybrid capacitive deionisation. Desalination 436, 8–14.
Simons, B., Andersen, J.C.Ø., Shail, R.K., Jenner, F.E., 2017. Fractionation of Li, Be, Ga, Nb, Ta, in, Sn, Sb, W and Bi in the peraluminous early permian variscan granites of the cornubian batholith: precursor processes to magmatic-hydrothermal mineralisation. Lithos 278–281, 491–512.
Smeds, S.A., 1992. Trace elements in potassium-feldspar and muscovite as a guide in the prospecting for lithium- and tin-bearing pegmatites in Sweden. J. Geochem. Explor. 42 (Issues 2–3), 351–369.
Smith, J.V., 1974. The Feldspar Minerals 2: Chemical and Textural Properties. Springer-Verlag, Heidelberg, Germany, p. 690.
Srivastava, P.K., Namga, S., Singh, P., Arora, N., Magotra, R., 2018. Hydrothermal chloritisation in granitoids of chumathang, ladakh. Int. J. Earth Sci. Eng. 11 (No. 01), 75–80.
Sun, S., Yu, X., Li, M., Duo, J., Guo, Y., Deng, T., 2020. Green recovery of lithium from geothermal water based on a novel lithium iron phosphate electrochemical technique. J. Clean. Prod. 247, 119178.
Sweetapple, M.T., Tassios, S., 2015. Laser-induced breakdown spectroscopy (LIBS) as a tool for in situ mapping and textural interpretation of lithium in pegmatite minerals. Am. Mineral. 100, 2141–2151.
Szanyi, J., Kovács, B., 2010. Utilisation of geothermal systems in South-East Hungary. Geothermics 39, 357–364.
Szederkényi, T., 1997. Basic lithostratigraphic units of Hungary. Charts and short descriptions. Paleozoic II. Hung. Geol. Survey 29, 65–69.
Szemerédi, M., Varga, A., Szepesi, J., Pál-Molnár, E., Lukács, R., 2020. Lavas or ignimbrites? Permian felsic volcanic rocks of the Tisza Mega-unit (SE Hungary) revisited: a petrographic study. Cent. Eur.Geol. 63/1, 1–18.
Ustaszewski, K., Schmid, S.M., Lugović, B., Schuster, R., Schaltegger, U., Bernoulli, D., Hottinger, L., Kounov, A., Fügenschuh, B., Schefer, S., 2009. Late Cretaceous intra-oceanic magmatism in the internal Dinarides (northern Bosnia and Herzegovina): implications for the collision of the Adriatic and European plates. Lithos 108, 106–125.
Varsányi, I., Kovács, L.Ó., 2005. The role of groundwater flow in controlling the arsenic concentration in the southern part of the Great Hungarian Plain. Acta Minerol.-Petrogr. (Szeged) 46, 47–52.
Vass, I., Tóth, T.M., Szanyi, J., Kovács, B., 2018. Hybrid numerical modelling of fluid and heat transport between the overpressured and gravitational flow systems of the Pannonian Basin. Geothermics 72, 268–276.
Vikström, H., Davidsson, S., Höök, M., 2013. Lithium availability and future production outlooks. Appl. Energy 110, 252–266.
Villaros, A., Pichavant, M., 2019. Mica-liquid trace elements partitioning and the granite-pegmatite connection: the St-Sylvestre complex (Western French Massif Central). Chem. Geol. 528, 119265.
Vu, H., Bernardi, J., Jandová, J., Vaculíková, L., Goliáš, V., 2013. Lithium and rubidium extraction from zinnwaldite by alkali digestion process: sintering mechanism and leaching kinetics. Int. J. Miner. Process. 123, 9–17.
Whitney, D.L., Evans, B.W., 2010. Abbreviations for names of rock-forming minerals. Am. Mineral. 95 (1), 185–187.
White, W.M., 2013. Geochemistry. John Wiley & Sons Inc.
Wilkinson, J.J., Chang, Z., Cooke, D.R., Baker, M.J., Wilkinson, C.C., Inglis, S., Chen, H., Gemmel, J.B., 2015. The chlorite proximitor: a new tool for detecting porphyry ore deposits. J. Geochem. Explor. 152, 10–26.
Wise, M.A., Harmon, R.S., Curry, A., Jennings, M., Grimac, Z., Khashchevskaya, D., 2022. Handheld LIBS for Li exploration: an example from the carolina tin-spodumene belt, USA. Minerals 12 (1), 77.
Wisniewska, M., Fijałkowska, G., Ostolska, I., Franus, W., Nosal- Wiercinska, A., Tomaszewska, B., Goscianska, J., Wójcik, G., 2018. Investigations of the possibility of lithium acquisition from geothermal water using natural and synthetic zeolites applying poly(acrylic acid). J. Clean. Prod. 195, 821–830.
Zhang, J.-W., Zhao, Z.-Q., Yan, Y.-N., Cui, L.-F., Wang, Q.-L., Meng, J.-L., Li, X.-D., Liu, C.-Q., 2021. Lithium and its isotopes behavior during incipient weathering of granite in the eastern Tibetan Plateau, China. Chem. Geol. 559, 119969.
Zilahi-Sebess, L., Gyuricza, Gy, 2013. Battonya geotermikus koncesszióra javasolt terület komplex érzékenységi és terhelhetőségi vizsgálati jelentése – complex sensitivity and resilience of the Battonya area proposed for geothermal concession. Min.Geol. Surv. Hung. 185.